JOURNAL OF SOLID STATE CHEMISTRY **132,** 47–55 (1997)
ARTICLE NO. SC977406

The Potassium Aluminum Phosphate $KAl(HPO_4)_2 \cdot H_2O$: X-Ray Diffraction, Neutron-Scattering, and Solid-State NMR Characterization

Stefan Dick, Ursula Goßner, and Armin Weiss

Institut für Anorganische Chemie der Universität München, Meiserstrasse 1, 80333 Müunchen, Germany

Christian Robl

Institut für Anorganische und Analytische Chemie der Universität Jena, August-Bebel-Strasse 6-8, 07743 Jena, Germany

Gisbert Grossmann and Gisela Ohms

Institut für Analytische Chemie der TU Dresden, Mommsenstrasse 13, 01062 Dresden, Germany

and

Manfred Müller

Hahn-Meitner-Institut Berlin, Glienickerstrsse 100, 14109 Berlin, Germany

Received December 23, 1996; in revised form March 24, 1997; accepted April 2, 1997

The 1:1:2 potassium aluminum phosphate $KAl(HPO_4)_2 \cdot H_2O$ has been synthesized and characterized by single-crystal X-ray diffraction. The compound crystallizes in the monoclinic space group $P2_1/c$ with $Z=8$. Crystal data: $a=1004.0(2)$ pm, $b=910.7(2)$ pm, $c=1625.4(3)$ pm, $\beta=100.98(2)^\circ$, $R_g=0.044$. A neutron-scattering experiment with subsequent refinement of the powder pattern of $KAl(DPO_4)_2 \cdot D_2O$ elucidated the D atom positions in the deuterated compound. Crystal data: $a=1003.7(1)$ pm, $b=910.5(1)$ pm, $c=1622.3(2)$ pm, $\beta=100.97(1)^\circ$, $R_{wp}=0.044$. The structure consists of two different AlO_6-octahedra and four different HPO_4^{2-} tetrahedra. Corner sharing between these polyhedra creates a complicated three-dimensional framework with K^+ in cavities. Building units of that framework are Al phosphate chains that form various interconnections by corner sharing of polyhedra and hydrogen bonds. The hydrogen-bond donor and acceptor properties of the phosphates and water molecules are discussed along with their function in the structure. ^{31}P solid-state MAS spectra show only three δ_{iso} values at -6.5, -10.7 and -12.6 ppm instead of the expected four different isotropic chemical shifts. The sideband system at -10.7 ppm has twice the intensity of each of the outer systems. Considering the surroundings of the four HPO_4^{2-} tetrahedra it can be assumed that the first δ_{iso} value results from P(4), the second from P(2) and P(3), and the third from P(1). Significant differences between a given value of the principal axes σ_{ii} of the nuclear magnetic shielding tensors of the phosphorus atoms are observed only for σ_{11} of P(4) being more deshielded and for σ_{22} of P(1) being more shielded.

INTRODUCTION

In the recent years we studied the reactions of clay minerals with K^+ and phosphate solutions under various conditions and were able to identify a couple of crystalline products (taranakite, minyulite, $KAl(HPO_4)_2 \cdot H_2O$, $KAl_2(PO_4)_2(OH) \cdot 2H_2O$ (orthorhombic), $KAl_2(PO_4)_2(OH) \cdot 2H_2O$ (monoclinic)). Three of them—taranakite $K_3Al_5H_6(PO_4)_8 \cdot 18H_2O$, minyulite $KAl_2(PO_4)_2(OH) \cdot 4H_2O$, and $KAl(HPO_4)_2 \cdot H_2O$—could be characterized by single-crystal X-ray structure analysis (1–3). The latter phase is the product of phosphate degradation of clay minerals like kaolinite, halloysite, and montmorillonite at pH 2 and temperatures above 363 K.

The interaction of clay minerals with phosphate-containing solutions is of great interest because the long-time stability of waste deposits sealed with clays is limited by reactions of those materials with leachates from the landfills. Combination of anaerobic and aerobic biological waste degradation can create favourable conditions for the transformation of these minerals, thus destroying their sealing properties. It is therefore necessary to determine the conditions (pH, temperature, concentrations, time, counterions) for transformations and the products which substitute the original clay. Chemical and physical properties, e.g., crystal structure, intercalation properties and crystal habit, decide whether the products let waste water permeate from the deposit and

0022-4596/97 $25.00

give rise to a contamination of deeper groundwater levels. The conditions for the formation of $KAl(HPO_4)_2 \cdot H_2O$, however, are likely to occur in waste deposits only in very special circumstances.

In the past years insoluble aluminum phosphates find a growing interest as precursors or additives in phosphate-containing bioceramics. In addition, aluminum orthophosphates, $AlPO_4$, and modified products are characterized by solid-state NMR with respect to their catalytic properties (4–7). In this paper we present a complete single-crystal X-ray structure determination of $KAl(HPO_4)_2 \cdot H_2O$. To our knowledge this phosphate has not yet been found in nature. Its synthesis from $AlCl_3$ was described for the first time by Haseman *et al.* in their semial contribution about K–Al and K–Fe phosphates (8). Smith and Brown performed the first single-crystal X-ray diffraction experiments and concluded the monoclinic space group $P2_1/c$ (9).

Since hydrogen bonds seem to play an important role in stabilizing the structure of compounds of that type we performed an additional powder neutron-scattering experiment with $KAl(DPO_4)_2 \cdot D_2O$ in order to elucidate the D atom positions. Solid-state ^{31}P NMR MAS spectroscopy has been used as a supplementary method for the investigation of the microstructure around the phosphorus atoms.

EXPERIMENTAL

Synthesis

A 1:1 mixture (20 ml) of 1 molar aqueous solutions of KH_2PO_4 and H_3PO_4 was filled in a glass ampoule and mixed with 0.5 g gibbsite (Merck). The ampoule was heated at 418 K for 30 days and then cooled to room temperature at 5 K/h. The product was filtered off, washed with water, rinsed with ethanol, and air dried. The product consisted of small transparent colorless rod-like crystals of $KAl(HPO_4)_2 \cdot H_2O$ and powder of the same material.

As starting material for the synthesis of the fully deuterated analogue D_3PO_4 was prepared form D_2O (99.5% D, Aldrich) and P_4O_{10}, KD_2PO_4 from D_3PO_4 and KOD (99.5% D, Aldrich), and $Al(OD)_3$ from Al foil and D_2O. Powder of $KAl(DPO_4)_2 \cdot D_2O$ was then synthesized by hydrothermal reaction of $Al(OD)_3$ with phosphate solution as described above.

Single Crystal X-Ray Diffraction

A crystal of $KAl(HPO_4)_2 \cdot H_2O$ with dimensions $0.06 \times 0.02 \times 0.24$ mm^3 was selected for indexing and intensity data collection on a Siemens R3m/V four-circle diffractometer using monochromatized Mo$K\alpha$ radiation. Intensity data were corrected for Lp and absorption effects. Corrections for absorption effects were based on indexed faces of the crystal. On the basis of systematic absences the space group was determined to be $P2_1/c$ in agreement with earlier work (9). Direct methods were used to locate the metal and phosphorus atoms, while the positions of O and H atoms were found in difference Fourier maps. The structure model was refined by full-matrix least-squares refinement minimizing $w(|F_o| - |F_c|)^2$. All nonhydrogen atoms were refined with anisotropic, H atoms with one common isotropic displacement coefficient. Corrections for anomalous dispersion and secondary extinction were applied. Calculations were performed with the program system SHEXTL-Plus (10) on a MicroVAX II. Further details of the crystal structure determination are available from the Fachinformationszentrum Karlsruhe, Eggenstein-Leopoldshafen, Germany, on quoting the depository number CSD-406182, the names of the authors and the journal citation.

Powder Neutron Scattering

A neutron powder diffractogram of $KAl(DPO_4)_2 \cdot D_2O$ was measured at the Hahn-Meitner-Institut Berlin on the powder diffractometer E3 (research proposal CHE-01-158). A wavelength of about 240 pm was selected with a pyrographite monochromator. The exact wavelength of $\lambda = 244.52$ pm was calibrated against a recorded diffractogram of α-Fe at room temperature and the known lattice constant of that sample. Diffraction data were recorded with a $^{10}BF_3$ multidetector in a 2θ range from 11.2 to 90.0° within 38000 s. The data were corrected for detector cell efficiencies after measuring the scattered intensity of a vanadium sample.

Rietveld analysis of the obtained diffractogram was performed with the program PROFIL (11) on a SGI Indy workstation. As a starting model cell constants and atomic parameters from the X-ray structure determination of $KAl(HPO_4)_2 \cdot H_2O$ were used. Background intensity was estimated graphically and modeled by eight background points. After refinement of scale factor, diffractometer shift, cell constants, an asymmetry parameter for gaussian peak shape, and resolution parameters (u, v, w) R_{wp} had dropped to 0.15. A further decrease of R_{wp} was achieved by additional refinement of positions and isotropic displacement parameters of D atoms, while all parameters of non-D atoms were kept fixed. With 42 parameters refinement converged at $R_{wp} = 0.044$.

NMR Spectroscopy

The ^{31}P high power ^1H decoupled solid-state MAS NMR spectra were recorded at 121.5 MHz using a Bruker MSL 300 spectrometer at spinning frequencies of 2.0 and 2.7 kHz. The 90° pulse lengths were 5 μs, repetition times of 10 or 100 s were used for spectra with cross-polarization (CP) or without this, respectively. The CP spectra were measured

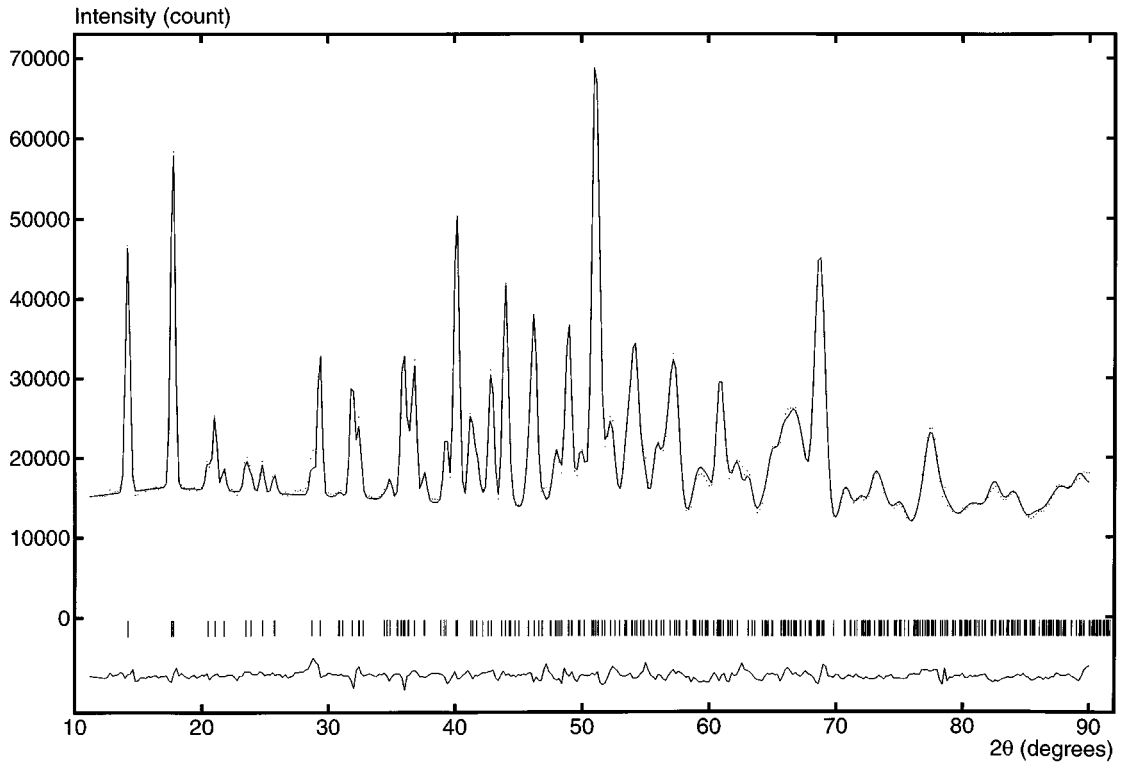

FIG. 1. Observed, calculated, and difference profiles for powder neutron diffraction of $KAl(DPO_4)_2 \cdot D_2O$. Vertical tick marks indicate calculated reflection positions.

with a cross polarization time of 2 ms using a pulse sequence containing two contact pulses (12).

The ^{31}P chemical shifts are relative to 85% H_3PO_4. The principal values of the chemical shift tensor have been computed by means of the program WIN-MAS (13) using intensities and widths of the lines of the resolved spinning sideband systems. The principal values of the absolute nuclear magnetic shielding tensor were calculated from the chemical shift tensor (14) with $\sigma_{ii} = 328$ ppm $- \delta_{ii}$ and have been labeled acording to the convention $\sigma_{33} \geq \sigma_{22} \geq \sigma_{11}$. The standard deviations of the isotropic chemical shifts and of the principal values are 0.1 ppm and 5 ppm, respectively.

RESULTS AND DISCUSSION

Crystal Structure of $KAl(HPO_4)_2 \cdot H_2O$

The data for the the single-crystal X-ray structure determination of $KAl(HPO_4)_2 \cdot H_2O$ are summarized in Table 1. Atomic coordinates and displacement parameters are listed in Table 2, and selected bond distances and angles are listed in Tables 3 and 4.

The structure of $KAl(HPO_4)_2 \cdot H_2O$ consists of two different types of AlO_6 octahedra around Al(1) and Al(2) and four crystallographically independent HPO_4^{2-} tetrahedra around P(1), P(2), P(3), and P(4). Corner sharing between these polyhedra creates a rather complicated three dimensional network with K^+ entrapped in cavities of the aluminum phosphate skeleton.

Al(1) is coordinated distorted octahedrally by four oxygen atoms of HPO_4^{2-} tetrahedra (P(1), $2 \times$ P(2), and P(3)) and two *cis* water molecules O(17) and O(18) (Fig. 2). The distances between Al(1) and O from phosphate are in the normal range for bonds of that type. As expected longer bonds are found between Al(1) and the water oxygens. Nevertheless, the bond between Al(1) and O(18) is with a length of only 193.2 pm unusual short. The coordination sphere of Al(2) is again distorted octahedral but made up of only oxygen from HPO_4^{2-} (P(1), P(2), $2 \times$ P(3), and $2 \times$ P(4)) (Fig. 3). The Al–O distances span a rather wide interval from about 186 to 194 pm.

The HPO_4^{2-} tetrahedra (Fig. 4) can be divided into two groups: In one type (P(2) and P(3)) three oxygen corners of the tetrahedra are connected with Al while one oxygen atom is protonated. In that way P(2) is connected with $2 \times$ Al(1) and Al(2) via oxygen, and P(3) is connected with $2 \times$ Al(2) and Al(1). In the second type of tetrahedra (P(1) and P(4)) there is again one protonated oxygen but only two corners link to Al leaving a formally free corner. While phosphate P(1) is connected with both Al(1) and Al(2), phosphate P(4) is linked to $2 \times$ Al(2) only.

TABLE 1
Summary of Data for the Single-crystal X-Ray Structure Determination of $KAl(HPO_4)_2 \cdot H_2O$

Formula	$KAl(HPO_4)_2 \cdot H_2O$
Crystal color	Colorless
Crystal size	$0.06 \times 0.02 \times 0.24$
Formula mass	276.1
Space group	$P2_1/c$
Lattice constants	$a = 1004, 2(2)$ pm
	$b = 910, 7(2)$ pm
	$c = 1625, 4(3)$ pm
	$\beta = 100, 98(2)^\circ$
	$V = 1459.0(5) \times 10^6$ pm^3
Z	8
$\rho_{calc.}$	2.514 g·cm^{-3}
μ(Mo$K\alpha$)	1.296 mm^{-1}
Scan mode/scan width	ω-2θ/1.0°
Scan speed	0.92–7.32°/min
2θ-range	5–60°
Independent reflections	4295 (of 4771)
Observed reflections	2782
With $\lvert F_o\rvert \geq 3\sigma\lvert F_o\rvert$	($R_{int} = 0.033$)
Min./max. transmission	0.9166/0.9735
Extinction parameter[a]	$\chi = 0.00013(4)$
Parameters refined	261
Residuals[b] $R/R_w/R_g$	0.0731/0.0513/0.0442
Weighting scheme	$1/\sigma^2_{\lvert F_o\rvert}$
Maxima in last	$+1.11/-1.11\ e \times 10^{-6}$ pm^{-3}
Difference Fourier synthesis	

[a] $|F_o^\star| = |F_o|[1 + 0.002\chi|F_o|^2/\sin(2\theta)]^{-1/4}$.

[b] $R = \dfrac{\sum||F_o| - |F_c||}{\sum|F_o|}$; $R_w = \dfrac{\sum\sqrt{w}||F_o| - |F_c||}{\sum\sqrt{w}|F_o|}$; $R_g = \sqrt{\dfrac{\sum(w(|F_o| - |F_c|)^2}{\sum(w|F_o|^2)}}$.

TABLE 2
Atomic Coordinates ($\times 10^4$) and Equivalent Displacement Coefficients ($pm^2 \times 10^{-1}$) for $KAl(HPO_4)_2 \cdot H_2O$

Atom	x	y	z	U_{eq}[a]
K(1)	11122(2)	4441(2)	3885(1)	19(1)
K(2)	7703(2)	6568(2)	2707(1)	24(1)
Al(1)	14124(2)	8125(2)	3053(1)	9(1)
Al(2)	9283(2)	813(2)	3500(1)	7(1)
P(1)	7169(2)	3320(2)	3896(1)	10(1)
P(2)	13591(2)	4832(2)	2611(1)	8(1)
P(3)	10992(2)	8046(2)	3036(1)	8(1)
P(4)	11677(2)	1343(2)	5090(1)	8(1)
O(1)	5992(4)	3219(6)	4346(3)	25(2)
O(2)	8246(5)	4486(6)	4348(3)	24(2)
O(3)	6736(4)	3856(5)	2989(2)	12(1)
O(4)	7954(4)	1875(5)	3977(2)	12(1)
O(5)	14346(4)	6276(4)	2626(3)	13(1)
O(6)	14170(4)	3725(5)	2068(3)	14(1)
O(7)	12067(4)	4945(5)	2320(2)	12(1)
O(8)	13705(5)	4182(5)	3518(3)	17(1)
O(9)	10241(4)	71277(5)	3657(3)	15(1)
O(10)	12485(4)	7783(5)	3360(2)	11(1)
O(11)	10602(4)	9654(4)	3054(3)	10(1)
O(12)	10486(4)	7393(4)	2182(3)	11(1)
O(13)	12746(5)	118(5)	4972(3)	16(1)
O(14)	12443(4)	2743(5)	5387(3)	15(1)
O(15)	10894(4)	745(5)	5742(2)	10(1)
O(16)	10735(4)	1625(5)	4268(2)	10(1)
O(17)	13945(5)	10178(5)	3571(3)	18(1)
O(18)	14912(5)	7494(6)	4175(3)	18(1)
H(11)	4675(74)	10698(84)	3642(43)	32(8)
H(12)	3722(73)	10129(77)	4070(44)	32(8)
H(21)	4444(68)	7261(77)	4626(43)	32(8)
H(22)	14297(72)	2580(80)	5820(46)	32(8)
H(1)	7855(73)	5326(79)	4381(43)	32(8)
H(2)	4424(71)	4036(84)	3828(43)	32(8)
H(3)	10227(68)	1945(81)	5981(41)	32(8)
H(4)	12700(81)	−483(87)	5213(46)	32(8)

[a] U_{eq} is defined as a third of the trace of the orthogonalized U_{ij} tensor.

As expected in all phosphate tetrahedra the distances between P and the protonated O are the longest, whereas shortened distances are found between P and the "free" oxygens O(1) and O(14) with formal double-bond character.

The three-dimensional framework of $KAl(HPO_4)_2 \cdot H_2O$ can be seen as being built of interconnected infinite chains of alternate corner sharing AlO_6 octahedra and $PO_3(OH)$ tetrahedra running parallel to the *a* axis and the *c* axis (Fig. 5). The chain parallel to *a* consists of only Al(1) octahedra which are connected by *cis*-coordinated P(2) tetrahedra (Fig. 2). Across that chain parallel to *c* runs another chain of only Al(2) octahedra. These octahedra are linked to dimers by two *cis* O(4) tetrahedra (Fig. 3); the dimers themselves are connected to chains by P(3) tetrahedra. Interconnections between the two chain systems are established by P(1), P(2) and P(3) tetrahedra and, in addition, by hydrogen bonds.

Two crystallographically independent K^+-ions are situated in channel-like cavities of the framework. Counting only K–O distances up to 340 pm K(1) is coordinated by nine oxygen atoms from phosphate tetrahedra only; K(2) has coordination number 11 and forms the shortest contact with water O(17).

Hydrogen Bonding in $KAl(DPO_4)_2 \cdot D_2O$

The structure of $KAl(DPO_4)_2 \cdot D_2O$ contains eight different D atoms, seven of which are involved in hydrogen bonds. These atoms bind to phosphate tetrahedra and water molecules. O–D distances and O–D–O angles as determined by neutron scattering (cf. Tables 5 and 6 for crystallographic data and atomic coordinates) are summarized in Table 7. As mentioned above, the four different phophate tetrahedra can be divided in two groups regarding their connections with Al octahedra. The same division can be made regarding the coordination of D atoms.

Phosphates P(2) and P(3) each form only one rather long bond of about 105 pm to D(2) and D(3) via O(8) and O(9),

TABLE 3
Selected Bond Lengths (pm) in $KAl(HPO_4)_2 \cdot H_2O$

Al(1)–O(10)	184.4(5)	Al(2)–O(12)	185.9(4)
Al(1)–O(6)	184.4(5)	Al(2)–O(16)	188.1(4)
Al(1)–O(5)	185.1(5)	Al(2)–O(7)	188.4(4)
Al(1)–O(3)	187.0(4)	Al(2)–O(15)	190.9(4)
Al(1)–O(18)	193.2(5)	Al(2)–O(4)	192.6(4)
Al(1)–O(17)	207.2(5)	Al(2)–O(11)	193.9(4)
P(1)–O(1)	150.7(5)	P(4)–O(16)	150.5(4)
P(1)–O(4)	152.7(4)	P(4)–O(14)	151.9(4)
P(1)–O(3)	153.5(4)	P(4)–O(15)	153.5(5)
P(1)–O(2)	159.2(5)	P(4)–O(13)	158.5(5)
P(2)–O(5)	151.5(4)	P(3)–O(12)	150.6(4)
P(2)–O(7)	151.7(4)	P(3)–O(10)	151.1(4)
P(2)–O(6)	152.6(5)	P(3)–O(11)	151.7(4)
P(2)–O(8)	157.3(5)	P(3)–O(9)	158.3(5)
K(1)–O(9)	264.6(5)	K(2)–O(17)	271.1(5)
K(1)–O(16)	265.8(4)	K(2)–O(3)	272.4(4)
K(1)–O(8)	278.0(5)	K(2)–O(9)	277.2(4)
K(1)–O(12)	283.2(4)	K(2)–O(6)	279.1(5)
K(1)–O(7)	291.5(5)	K(2)–O(11)	287.6(5)
K(1)–O(14)	298.0(4)	K(2)–O(7)	308.5(5)
K(1)–O(2)	298.6(5)	K(2)–O(12)	316.4(5)
K(1)–O(2)	312.0(6)	K(2)–O(14)	319.2(5)
K(1)–O(11)	329.9(4)	K(2)–O(2)	323.3(5)
		K(2)–O(8)	325.0(5)
		K(2)–O(5)	335.9(5)

TABLE 4
Selected Bond Angles (°) in $KAl(HPO_4)_2 \cdot H_2O$

O(1)–P(1)–O(2)	110.1(3)	O(5)–P(2)–O(6)	109.8(3)
O(1)–P(1)–O(3)	112.4(2)	O(5)–P(2)–O(7)	114.7(2)
O(1)–P(1)–O(4)	110.2(3)	O(5)–P(2)–O(8)	111.3(2)
O(2)–P(1)–O(3)	106.0(3)	O(6)–P(2)–O(7)	109.7(2)
O(2)–P(1)–O(4)	103.9(2)	O(6)–P(2)–O(8)	109.0(3)
O(3)–P(1)–O(4)	113.9(2)	O(7)–P(2)–O(8)	101.9(3)
O(9)–P(3)–O(10)	105.1(2)	O(13)–P(4)–O(14)	108.4(3)
O(9)–P(3)–O(11)	108.3(3)	O(13)–P(4)–O(15)	106.4(3)
O(9)–P(3)–O(12)	105.8(2)	O(13)–P(4)–O(16)	109.8(3)
O(10)–P(3)–O(11)	112.9(2)	O(14)–P(4)–O(15)	112.0(2)
O(10)–P(3)–O(12)	113.3(2)	O(14)–P(4)–O(16)	109.4(2)
O(11)—P(3)–O(12)	110.9(2)	O(15)–P(4)–O(16)	110.8(2)
O(5)–Al(1)–O(10)	97.2(2)	O(4)–Al(2)–O(16)	92.5(2)
O(5)–Al(1)–O(17)	177.6(2)	O(4)–Al(2)–O(7)	92.0(2)
O(5)–Al(1)–O(18)	91.5(2)	O(4)–Al(2)–O(11)	177.0(2)
O(5)–Al(1)–O(3)	93.0(2)	O(4)–Al(2)–O(12)	91.5(2)
O(5)–Al(1)–O(6)	92.8(2)	O(4)–Al(2)–O(15)	87.5(2)
O(10)–Al(1)–O(17)	83.3(2)	O(16)–Al(2)–O(7)	175.3(2)
O(10)–Al(1)–O(18)	85.4(2)	O(16)–Al(2)–O(11)	87.9(2)
O(10)–Al(1)–O(3)	93.3(2)	O(16)–Al(2)–O(12)	85.5(2)
O(10)–Al(1)–O(6)	168.2(2)	O(16)–Al(2)–O(15)	91.1(2)
O(17)–Al(1)–O(18)	86.4(2)	O(7)–Al(2)–O(11)	87.6(2)
O(17)–Al(1)–O(3)	89.2(2)	O(7)–Al(2)–O(12)	93.3(2)
O(18)–Al(1)–O(3)	174.8(2)	O(7)–Al(2)–O(15)	90.1(2)
O(17)–Al(1)–O(6)	86.0(2)	O(11)–Al(2)–O(12)	91.5(2)
O(18)–Al(1)–O(6)	88.1(2)	O(11)–Al(2)–O(15)	89.5(2)
O(3)–Al(1)–O(6)	94.4(2)	O(12)–Al(2)–O(15)	176.5(2)

respectively. These D atoms are involved in strong hydrogen bonds to phosphates P(1) and P(4) via O(1) and O(15). Long and short distances of D and O differ about 40%, while the coordination of D is not far from linear. The tetrahedra of this group do not act as acceptors of hydrogen bonds but only as donors; hydrogen bonds are formed only to phosphates of the second group of tetrahedra.

For tetrahedra P(1) and P(4) the situation is quite different. They exhibit shorter distances D(1)–O(2) and D(4)–O(13) and form longer hydrogen bonds to O(14) and O(4), respectively. Tetrahedra of this group are therefore connected

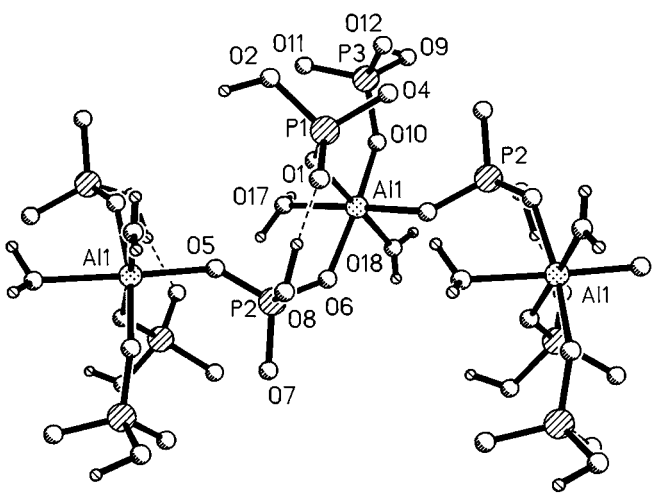

FIG. 2. Infinite chains of Al(1) and phosphate P(2) in $KAl(DPO_4)_2 \cdot D_2O$.

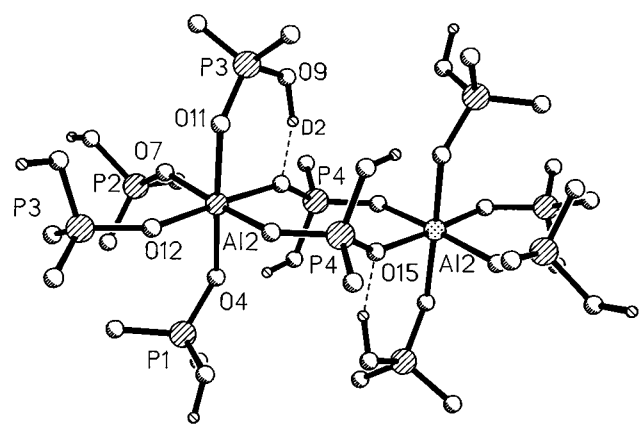

FIG. 3. Dimeric building unit of the Al(2) chains in $KAl(DPO_4)_2 \cdot D_2O$; the dimers are connected to chains by phosphate P(3).

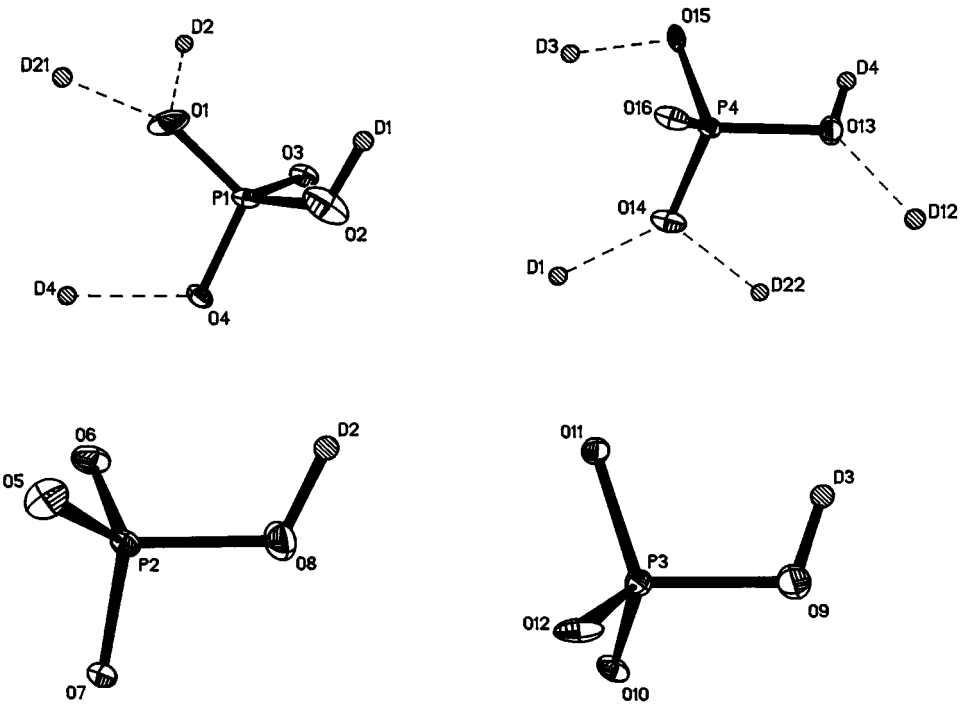

FIG 4. Hydrogen bonds to phosphates in $KAl(DPO_4)_2 \cdot D_2O$; thermal ellipsoides are plotted for a 50% probability level.

with each other by hydrogen bonds. In addition they act as acceptors for hydrogen bonds from tetrahedra P(2) and P(3) as stated above and from water molecules bound to Al(1). O(1) and O(14) with formal double bonds to P(1) and P(4), respectively, each form two hydrogen bonds in a way that O is coordinated distorted trigonal planar by the two D atoms and phosphorus. In addition, phosphate P(4) forms another hydrogen bond to water O(17) via D(12) therefore acting as a donor for one and an acceptor for four hydrogen bonds.

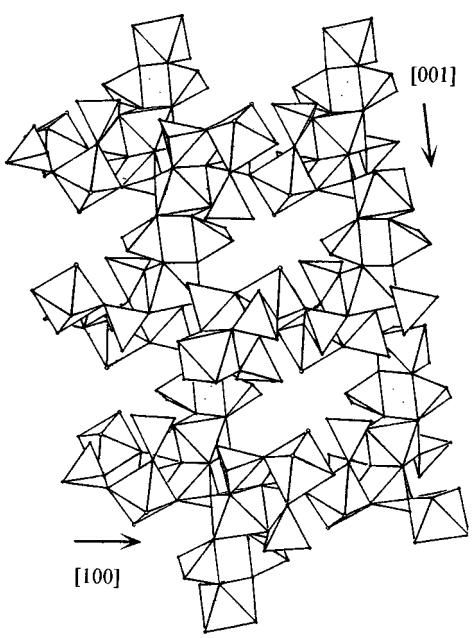

FIG. 5. Perspective view of the $KAl(HPO_4)_2 \cdot H_2O$ structure along the [010] direction; K atoms have been omitted for clarity.

TABLE 5
Summary of Data for Powder Neutron Diffraction of $KAl(DPO_4)_2 \cdot D_2O$

Formula	$KAl(DPO_4)_2 \cdot D_2O$
Formula mass	280.1
Space group	$P2_1/c$
Lattice constants	$a = 1003.7(1)$ pm
	$b = 910.5(1)$ pm
	$c = 1622.3(2)$ pm
	$\beta = 100.97(1)^\circ$
Z	8
2θ-range	11.2–90.0°
2θ-resolution	0.2°
Wavelength	$\lambda = 244.52$ pm
No. data points	395
No. reflections	280
No. parameters	42
Peak width parameters ($u/v/w$)	2.5(1)/ − 1.01(7)/0.25(1)
Residuals[a] $R_{exp}/R_I/R_{wp}$	0.017/0.035/0.044

[a] $R_{exp} = \sqrt{\frac{(N-P+C)}{\sum w y_{obs}^2}}$; $R_I = \frac{\sum |I_{obs} - I_{calc}|}{\sum I_{obs}}$; $R_{wp} = \sqrt{\frac{\sum w (y_{obs} - y_{calc})^2}{\sum w y_{obs}^2}}$ with $y_{obs} = y_{total}$ − background and $w = y_{obs}^{-1}$.

TABLE 6
Atomic Coordinates ($\times 10^4$) and Isotropic Displacement Coefficients ($pm \times 10^{-1}$) for D Atoms in $KAl(DPO_4)_2 \cdot D_2O$ as Determined by Neutron Powder Diffraction

Atom	x	y	z	U_{iso}
D(11)	4711(25)	10762(29)	3630(16)	26(9)
D(12)	3623(21)	10236(31)	4130(14)	42(9)
D(21)	4445(27)	7117(29)	4653(15)	88(15)
D(22)	14351(29)	2571(27)	5665(13)	37(9)
D(1)	7941(24)	5478(28)	4448(12)	15(8)
D(2)	4691(29)	3850(24)	3825(16)	51(13)
D(3)	10168(24)	2051(25)	5984(12)	67(13)
D(4)	12651(23)	-689(27)	5301(13)	53(11)

The two D atoms of water molecules also form one long and one short bond to O(17) and O(18), respectively. D(12) and D(21) with lengthened O–D bonds form hydrogen bonds to phosphate tetrahedra, while D(11) with its normal O–D bond length does not. Neither O(17) nor O(18) acts as a hydrogen bond acceptor.

During structure refinement D(22) was shifted to a position only 74 pm from O(18), a rather unlikely distance for an O–D bond. Attempts to move that atom to a position with a more reasonable O–D distance resulted in a dramatic increase of R_{wp} and unstable refinement. The short O–D distance, an unusual planar coordination of O(18) by D(21), D(22), and Al(1) and the comparatively strong anisotropic thermal motion of O(18) ($U_{11} = 7(2)$; $U_{22} = 27(3)$; $U_{33} = 18(2)\ pm^2 \times 10^{-1}$ as determined by X-ray diffraction) may indicate disorder of that water molecule. This interpretation is in addition supported by the short-distance O(18)–Al(1).

Hydrogen bonds between different phosphate tetrahedra as well as between phosphate and water seem to play an important role in the structure of $KAl(DPO_4)_2 \cdot D_2O$. For example, the chain of Al(1) and phosphate P(2) is accompanied by the hydrogen bond O(8)–D(2)–O(1) (Fig. 2). In a similar way the chain of Al(2) and phosphate P(4) is stabilized by O(4)–D(4)–O(14) (Fig. 3). In addition there are hydrogen bonds between different chains, and phosphate P(4) plays a remarkable role for that. Via the hydrogen bonds of O(14) it links a water molecule and a phosphate P(1) of the *same* Al(1) chain and via O(13) a phosphate P(1) of *another* Al(1) chain. A second Al(2)–chain is connected via the hydrogen acceptor function of O(15).

TABLE 7
Interatomic Distances and Angles of D Atoms in $KAl(DPO_4)_2 \cdot D_2O$ as Determined by Neutron Poweder Diffraction

	O–D ··· O		O–D [pm]	O ··· D [pm]	Angle O–D ··· O [°]
O(2)	**D(1)**	O(14)	98(3)	170(3)	175(2)
O(8)	**D(2)**	O(1)	106(3)	153(3)	171(3)
O(9)	**D(3)**	O(15)	105(2)	149(2)	162(2)
O(13)	**D(4)**	O(4)	93(3)	178(3)	161(2)
O(17)	**D(11)**		92(3)		
O(17)	**D(12)**	O(13)	102(2)	176(2)	167(2)
O(18)	**D(21)**	O(1)	104(3)	179(3)	164(2)
O(18)	**D(22)**	O(14)	74(3)	189(3)	173(2)

^{31}P *Solid-State NMR Spectroscopy*

The results of the solid-state NMR investigations are summarized in Fig. 6 and Table 8. Although the X-ray diffraction analysis yields four crystallographically independent phosphorus atoms with different P–O distances and O–P–O angles (cf. Tables 3 and 4) the MAS spectra show only three different sideband systems. The sideband system at the isotropic chemical shift of -10.7 ppm has twice the intensity of each of the outer systems. This unexpected result implies that the set of principal values σ_{ii} calculated from the line intensities of this sideband system is a mean of two different sets of two phosphorus sites. It is therefore not useful to assign the sideband systems to the crystallographically different phosphorus sites by considering the tensor properties of the middle sideband system. The only

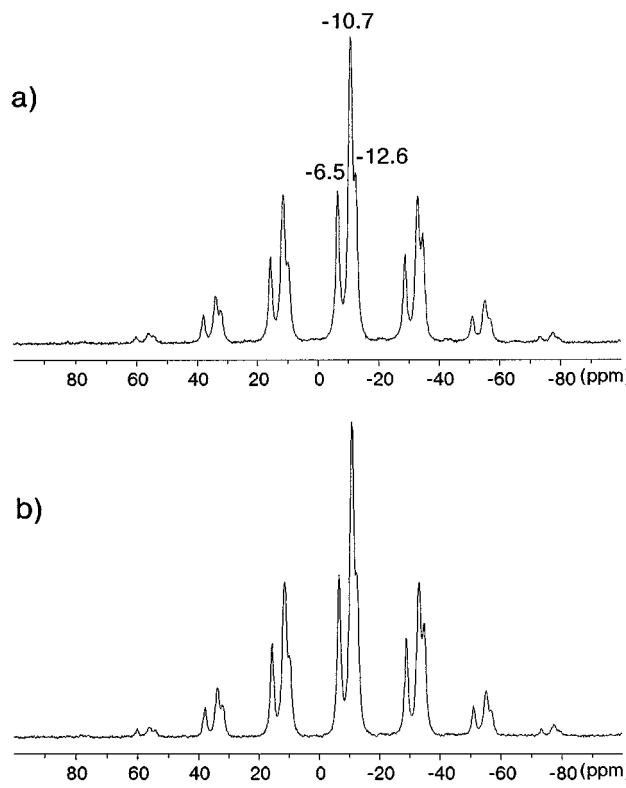

FIG. 6. ^{31}P MAS NMR spectra of $KAl(HPO_4)_2 \cdot H_2O$ at 121.5 MHz: (a) without cross-polarization and (b) with cross-polarization.

TABLE 8

^{31}P Isotropic Chemical Shifts δ_{iso} and Principal Values σ_{ii} (in ppm) of the Absolute Nuclear Magnetic Shielding Tensors for the Phosphorus Atoms of $KAl(HPO_4)_2 \cdot H_2O$

Atoms	δ_{iso}	σ_{11}	σ_{22}	σ_{33}
P(I)	−6.5	285	335	383
P(II)[b]	−10.7	293[c]	337[c]	386[c]
P(III)	−12.6	290	348	384

[a]The number of sideband systems corresponds to decreasing isotropic ^{31}P chemical shift.

[b]The intensity of this sideband system correponds to two crystallographically independent P atoms.

[c]Although the isotropic chemical shifts of two P atoms are distinguishable, the principal values σ_{ii} of the two tensors may be different. Therefore, these measured values must be considered as mean values.

significant differences of the principal values σ_{ii} of the nuclear magnetic shielding tensors obtained are a more deshielded value σ_{11} for P(I) and a more shielded value σ_{22} for P(III).

For phosphoryl compounds and orthophosphates many attempts are described in the literature (15–17) to find a correlation between the anisotropy $\Delta\sigma$ or the values σ_{ii} with P–O bond lengths or O–P–O angles. But all these correlation functions yield 2–5 times larger differences of the tensor properties than the experimental values of P(1) to P(4) show. Moreover, applying different functions changes the sequence of shielding of the four phosphorus atoms. Obviously neither the P–O bond lengths nor the O–P–O angles give an unambigous correlation to the chemical shift tensor properties. In practice the tensor properties of the phosphates are influenced by all atoms and ions surrounding the phosphorus atoms in first, second, and third spheres and one cannot expect that all changes in these spheres are straightforward reflected in the P–O bond lengths or the O–P–O angles.

TABLE 9

Number of Coordinted Atoms, Ions, and Hydrogen Bonds to the Oxygen Atoms Bonded to the Different Phosphorus Atoms

Coordinated atom	P(1) Al	P(1) K^+	P(1) HOR	P(2) Al	P(2) K^+	P(2) HOR	P(3) Al	P(3) K^+	P(3) HOR	P(4) Al	P(4) K^+	P(4) HOR
$O^{\delta-}$	1	1	-	1	1	-	1	1	-	1	1	-
$O^{\delta-}$	1	-	1	1	2	-	1	2	-	1	-	1
$O^{\delta-}$	-	-	2	1	-	-	1	-	-	-	2	2
O–H	-	2	-	-	2	-	-	2	-	-	-	1

^{31}P MAS spectra accumulated with and without cross-polarization (Fig. 6) show only small and not significant differences in the intensities of the sideband systems. Therefore these spectra do not provide additional information for the assignment of the isotropic shifts to the phosphorous sites P(1) to P(4). Although the P sites have different numbers of nearest protons (from 2 to 5 in a distance below 350 pm) the cross-polarization was of equal efficiency.

Furthermore, the empirical correlation between ^{31}P chemical shifts and the RO–P–OR bond angles proposed by Gorenstein (18) for phosphate esters is also not suited to solve this assignment problem.

If we assume that the number of bridged Al, coordinated K, and hydrogen bonds to each oxygen atom that surrounds the four phosphorus atom sites influences the isotropic chemical shift in a similar manner, we can make a suggestion for the assignment by comparison of the similarities and differences of coordination in the second sphere. In Table 9 equal numbers of coordinated atoms, ions, and hydrogen bonds to the oxygens of different phosphorus sites are marked by equal shading. The resulting assignment is: P(4) to P(I), P(2) and P(3) to P(II), and P(1) to P(III).

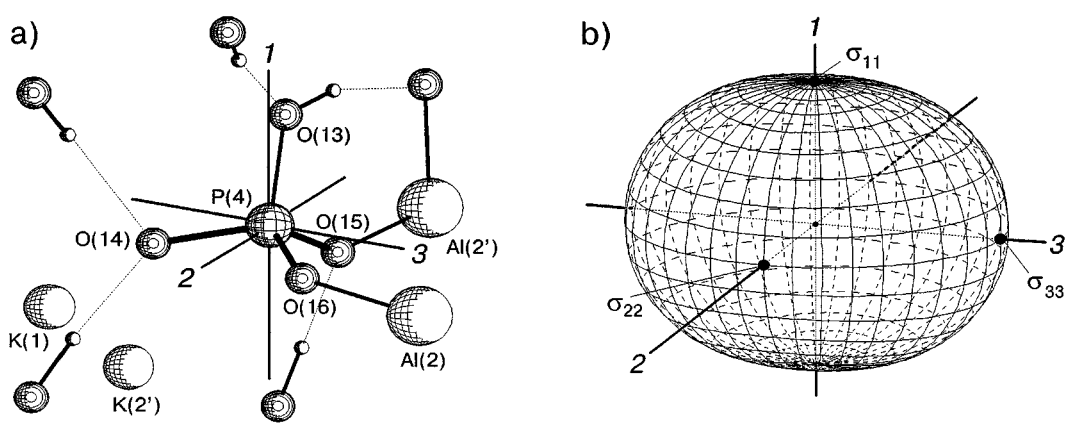

FIG. 7. ^{31}P nuclear magnetic shielding tensor of $KAl(HPO_4)_2 \cdot H_2O$. (a) Estimated orientation of the principal axes 1, 2, and 3 in the molecular framework; (b) ovaloid pictorial representation of the shielding tensor based on the principal values σ_{11}, σ_{22}, and σ_{33} of P(1).

Since the sideband system P(I) is well separated from the others its principal values of the nuclear magnetic shielding tensor are more accurate values than those of the overlapping sideband systems. Therefore it is useful to plot the ovaloid of the nuclear magnetic shielding (19) for atom P(4). This ovaloid is a surface showing the measurable shielding σ_{zz} as a function of the orientation of the principal axes to the direction of the magnetic field. If the direction of the magnetic field is parallel to one of the principal axes 1, 2, or 3, the nuclear magnetic shielding is equal to σ_{11}, σ_{22} and σ_{33}, respectively.

In Fig. 7 the microstructure of P(4) with the probable orientation of the principal axes and the ovaloid of the magnetic shielding tensor are shown. For the ovaloid calculation the experimental values σ_{ii} given on the absolute scale (14) must be used. The orientation of the principal axes to the molecular geometry was estimated on the base of experimental (20) and theoretical (21, 22) investigations of phosphates and can therefore somewhat differ from the true orientation.

ACKNOWLEDGMENT

Financial support of the neutron scattering experiments by the Berlin Neutron Scattering Center (BENSC) is gratefully acknowledged.

REFERENCES

1 U. Goßner, Dissertation, Universität Müunchen, 1995.
2. A. Weiß, U. Goßner, and Ch. Robl, *in* "Clays: Controlling the Environment" (G. J. Churchman, R. W. Fitzpatrick, and R. A. Eggleton, Eds.) Proc. 10th Int. Clay Conf., Adelaide, Australia, 1993, p. 253.
3. A. Weiß and U. Goßner, *in* "Clays and Clay Material Sciences" (A. Elsen, P. Grobet, M. Keung, H. Leeman, R. Schoonheydt, and H. Toufar, Eds.), Book of Abstracts, Euroclay 1995, Leuven, Belgium, p. 287.
4. W. A. Dollase, L. H. Merwin, and A. Sebald, *J. Solid State Chem.* **83,** 140 (1989).
5. S. Prabakar, K. J. Rao, and C. N. R. Rao, *Mater. Res. Bull.* **26,** 805 (1991)
6. J. Sanz, J. M. Campelo, and J. M. Marinas, *J. Catal.* **130,** 642 (1991).
7. B. Zibrowius, U. Lohse, and J. Richter-Mendau, *J. Chem. Soc. Faraday Trans.* **87,** 1433 (1991).
8. J. F. Haseman, J. R. Lehr, and J. P Smith, *Soil Sci. Soc. Am. Proc.* **15,** 76 (1950).
9. J. P. Smith and W. E. Brown, *Am. Mineralogist* **44,** 138 (1959).
10. G. M. Sheldrick, "SHELXTL-Plus Crystallographic System," Siemens Analytical X-Ray Instruments, Madison, WI, 1989.
11. J. Cockroft, PROFIL—A Rietveld Program... 5.17, 1994.
12. G. Jeschke and G. Grossmann, *J. Magn. Reson. Ser. A* **103,** 323 (1993).
13. WIN-MAS is available commercially from Bruker–Franzen Analytic GmbH, Fahrenheitsgasse 4, 28359 Bremen, Germany.
14. C. J. Jameson, A. C. de Dios, and K. Jameson, *Chem. Phys. Lett.* **167,** 575 (1990).
15. A-R. Grimmer, *Spectrochim. Acta A* **34,** 941 (1978).
16. G. L. Turner, K. A. Smith, R. J. Kirkpatrick, and E. Oldfield, *J. Magn. Reson.* **70,** 408 (1986).
17. S. Un and P. Klein, *J. Am. Chem. Soc.* **111,** 5119 (1989).
18. D. G. Gorenstein, *J. Am. Chem. Soc.* **97,** 898 (1975).
19. R. Radeglia, *Solid State NMR* **4,** 317 (1995).
20. S. J. Kohler, J. D. Ellet, and M. P. Klein, *J. Chem. Phys.* **64,** 4451 (1976).
21. F. R. Prado, C. Giessner-Prettre, B. Pullman, and J.-P. Daudey, *J. Am. Chem. Soc.* **101**, 1737 (1979).
22. N. E. Burlison, B. A. Dunel, and J. A. Ripmeester, *J. Magn. Reson.* **67,** 217 (1986)